

ADVANCED MATERIALS TECHNOLOGIES

Supporting Information

for *Adv. Mater. Technol.*, DOI 10.1002/admt.202401209

A Microfluidic Multiplex Sorter for Strain Development

*Chiara Leal-Alves, Sebastien Dumont, Zhiyang Deng, Sarah Alkhaldi, Ziuwin Leung, Michelle Oeser and Steve C. C. Shih**

Supplementary Information

A microfluidic multiplex sorter for strain development

Chiara Leal Alves^{1,2}, Sebastien Dumont³, Zhiyang Deng^{1,2}, Sarah Alkhaldi^{2,4}, Ziuwin Leung^{1,2},

Michelle Oeser³, Steve C.C. Shih^{1,2,4, §}

¹Department of Electrical and Computer Engineering, Concordia University, Montréal, Québec, Canada, H3B 1M8.

²Centre for Applied Synthetic Biology, Concordia University, Montréal, Québec, Canada, H4B 1R6.

³Lallemand Inc, Montreal, Quebec, Canada, H4P 2R2.

⁴Department of Biology, Concordia University, Montréal, Québec, Canada, HRB 1R6.

§Corresponding Author – steve.shih@concordia.ca

Supplementary Notes

Supplementary Note 1. Fluorescence measurements of droplets using Image J (Fiji)

Step 1: Image Input

1. File > Open... (Load image)
2. Image > Color > Split Channels
3. Select blue channel

Step 2: Adjusting Brightness and Contrast (B&C)

1. Image > Adjust > Brightness/Contrast... (Adjust B&C)
2. Use the adjustment sliders or click Auto to adjust the brightness and contrast.

Step 3: Measuring ROI (Background) Intensity

1. Select the Ellipse Tool from the toolbar or press E.
2. Draw an ROI (Region of Interest) over the background area.
3. Analyze > Measure (or press Ctrl+M).

Step 4: Subtracting Background Mean

1. Plugins > Math > Calculator Plus
2. Subtract Background Mean: Set the operation to Subtract and input the mean background intensity value measured in Step 3.

Step 5: Measuring ROI (Other Background) Regions

1. Repeat Step 3 for additional background regions to measure their intensity.

Step 6: Measuring ROI (Droplets) Intensity

1. Select the Ellipse Tool from the toolbar or press E.
2. Draw an ROI over a droplet.

3. Analyze > Measure (or press Ctrl+M).

Supplementary Note 2. Sample size calculations based on Cochran's equation for finite population.

These calculations were used to estimate the sample size from the mid- and high-level sorted population with 95% confidence level.

$$n_0 = \frac{z^2 \cdot p \cdot (1-p)}{e^2} \quad \text{Cochran's Equation for infinite population}$$

Where: n_0 = sample size for infinite population, $z = 1.96$ for 95% confidence level, p = fraction of the population exhibiting the trait, e = margin of error.

$$n = \frac{n_0}{1 + \frac{n_0 - 1}{N}} \quad \text{Cochran's Equation for finite population}$$

Where: n = the sample size for finite population, N = population size.

Case 1: Lowering the threshold that includes mid- and high-level strains (85-100% percentile) using binary sorting based on the histogram generated in Figure 4 and Table S3 for threshold gating and using IDY1 as sample calculation example.

Considering a $\pm 5\%$ margin of error and using a binary sorter at a lower threshold of 85% percentile:

- 1) Obtaining high-level strains (95% percentile) from recovered binary sorted strains.

The variable p represents *the proportion of the population that exhibits the trait*, in this case, high enzyme activity. To calculate p , we first determined number of droplets within the 95% percentile and the total within the binary sorting threshold ($> 85\%$ percentile) based on the histograms in Figure 4 and Table S3. We then calculated the Proportion of $> 95\%$ Percentile samples over the

sorted sample population as listed in Table S3. This value was subsequently multiplied by the binary sorting efficiency, which is approximately 90.2% (refer to Figure S6).

$e = 0.05$, $p = 0.3157$ and $N = 8145$ sorted droplets which is the amount of droplets sorted within the threshold of $> 85\%$ percentile (Figure 4 and Table S3).

$$n_0 = \frac{1.96^2 \cdot 0.3157 \cdot (1 - 0.3157)}{0.05^2} = 331.97 \approx 332$$

$$n = \frac{332}{1 + \frac{332-1}{8145}} = 319.03 \approx 320 \text{ samples}$$

2) Obtaining mid-level strains (85-95 % percentile) from recovered binary sorted strains.

The variable p represents *the proportion of the population that exhibits the trait*, in this case, mid enzyme activity. To calculate p , we first determined number of droplets within the 85-95% percentile and the total within the binary sorting threshold ($> 85\%$ percentile) based on the histograms in Figure 4 and Table S3. We then calculated the Proportion of 85-95% Percentile samples over the sorted sample population as listed in Table S3. This value was subsequently multiplied by the binary sorting efficiency, which is approximately 90.2% (refer to Figure S6).

$e = 0.05$, $p = 0.5863$, and $N = 8145$ sorted droplets which is the amount of droplets sorted within the threshold of $> 85\%$ percentile (Figure 4 and Table S3).

$$n_0 = \frac{1.96^2 \cdot 0.5863 \cdot (1 - 0.5863)}{0.05^2} = 372.72 \approx 373$$

$$n = \frac{373}{1 + \frac{373-1}{8145}} = 356.71 \approx 393 \text{ samples}$$

Case 2: Mid- and high-level strains (85-100% percentile) using multiplexed sorting (two thresholds) based on Figure 4 and Table S3 for threshold gating and using IDY1 as sample calculation example.

Considering a $\pm 5\%$ margin of error and using a multiplexed sorter (i.e. two thresholds):

- 1) Obtaining high-level strains (95% percentile) from the multiplexed sorted strains.

The variable p represents *the proportion of the population that exhibits the trait*, in this case, high enzyme activity. In this context, the proportion of samples exceeding the 95% percentile is determined solely by the efficiency of the multiplexed sorting, which is 98.6%, as shown in Figure 2.

$e = 0.05$, $p = 0.986$, and $N = 2833$ droplets which is the amount of droplets sorted within the threshold of $> 95\%$ percentile (Figure 4 and Table S3).

$$n_0 = \frac{1.96^2 \cdot 0.986 \cdot (1-0.986)}{0.05^2} = 21.21 \approx 22$$

$$n = \frac{22}{1 + \frac{22-1}{2833}} = 21.84 \approx 22 \text{ samples}$$

- 2) Obtaining mid-level strains (85-95 % percentile) from the multiplexed sorted strains.

The variable p represents *the proportion of the population that exhibits the trait*, in this case, mid enzyme activity. In this context, the proportion of samples from 85-95% percentile is determined solely by the efficiency of the multiplexed sorting, which is 98.6%, as shown in Figure 2.

$e = 0.05$, $p = 0.986$, and $N = 5312$ droplets which is the amount of droplets sorted within the threshold of 85-95% percentile (Figure 4 and Table S3).

$$n_0 = \frac{1.96^2 \cdot 0.986 \cdot (1-0.986)}{0.05^2} = 21.21 \approx 22$$

$$n = \frac{22}{1 + \frac{22-1}{5312}} = 21.91 \approx 22 \text{ samples}$$

Supplementary Note 3. Statistical analysis for picking colonies from plates

The analysis below was adapted from Shih et al.^[1].

$P_{wrong} = x$ where, P_{wrong} and x = are the probability of incorrect trait in the sub-populations

$P_{right} = 1 - x$ where, P_{right} = is the probability of correct trait in the sub-populations

Based on our simple size sample calculations we should assay at least 22 single mutant colonies, therefore, we chose to assay 24 colonies. To determine the worst-case scenario for failure of assaying the desired trait, we would have had at least 98.6% (sorting efficiency) chance of observing at least one incorrect mutant.

Given the failure probability x , the probability of having at least one out of $n=24$ mutants is mathematically:

$$1 - (1 - x)^n \geq 0.986, \text{ to solve for } x$$

$$(1 - x)^n \geq 1 - 0.986$$

$$(1 - x)^{24} \geq 0.014$$

$$(1 - x) \geq (0.014)^{\frac{1}{24}}$$

$$x \leq 1 - (0.014)^{\frac{1}{24}}$$

$$x \leq 1 - 0.8394$$

$$x \leq 0.1606$$

$x \leq 16\%$ chance of finding an incorrect trait in the population (worst case scenario)

Supplementary Note 4. Calculation for ethanol yield and concentration and fermentation efficiency

Based on the fermentation weight loss (CO₂ released from the reactor), from the mass balance from glucose to ethanol and carbon dioxide, we could calculate the ethanol content in the end of the fermentation:



For 2 mols of Ethanol generated, 2 mols of carbon dioxide is released, based on their molar mass:

$$MW_{\text{Ethanol}} = 46 \text{ g/mol}$$

$$MW_{\text{CO}_2} = 44 \text{ g/mol}$$

Conversion of mass of CO₂ to Ethanol is:

$$m_{\text{Ethanol}} = m_{\text{CO}_2} \cdot \frac{46\text{g}}{44\text{g}}$$

1- Calculation of theoretical ethanol conversion based on the sugar content in the synthetic media, which is ~ 0.555 g of sugar in the 3mL aliquots used for fermentation.

$$\text{Ethanol Conversion}_{\text{theoretical}}(g) = \frac{0.51\text{g Ethanol}}{\text{g of sugars}} \cdot 0.555 \text{ g of sugar} = 0.283\text{g Ethanol}$$

2- Experimental yield of ethanol over biomass.

$$Y_{\text{experimental}}(g) = \frac{m_{\text{Ethanol}}}{\text{biomass}}, \text{ where } m_{\text{ethanol}} \text{ is calculated based on CO}_2 \text{ release.}$$

3- Fermentation Efficiency calculated based on the mass of ethanol generated by fermentation over the ethanol theoretical conversion.

$$\text{Fermentation Efficiency}(\%) = 100\% \cdot \frac{m_{\text{Ethanol}}}{\text{Ethanol Conversion}_{\text{theoretical}}}$$

4- Ethanol volumetric concentration based on the conversion of ethanol mass to volume using density of 0.789g/mL, and the fermenters volume of 3 mL.

$$\text{Ethanol concentration } \left(\frac{v}{v} \% \right) = \frac{m_{\text{ethanol}}}{0.789 \cdot \text{Volume of media}}$$

Supplementary Tables

Table S1. Number of droplets produced and collected for the multiplexed efficiency assay. The ratio of droplets containing 0.1 mM fluorescein, 1 mM fluorescein, and PBS is 1:1:5, and the same total volume of droplets were generated for each specific volume.

Number of droplets in 50 μ L	Droplet volume (pL)		
	30	110	1,000
PBS	1,190,476	324,675	35,714
0.1 mM Fluorescein	238,095	64,935	7,143
1 mM Fluorescein	238,095	64,935	7,143
Total generated	1,666,667	454,545	50,000

Table S2. Calculated growth rates for diastatic yeast growing in different droplet volumes based on the logistic growth model, where r is the rate constant and YM is the maximum population.

IDY1			IDY2		
Droplet size (pL)	r (h^{-1})	YM (cells/droplet)	Droplet size (pL)	r (h^{-1})	YM (cells/droplet)
1000	0.096	9.25	1000	0.06	7.00
110	0.05	5.83	110	Unstable *	4.53
30	0.037	5.37	30	0.091	4.01

Table S3. Descriptive statistics of histogram of two diastatic yeast mutant population based in the droplet's fluorescence data.

Analysis	IDY1	IDY2
Total sample size	55603	45034
85%-95% Percentile sample size (Figure 4)	5312	4244
>95% Percentile sample size (Figure 4)	2833	2406
Sorted sample population size	8145	6650
85% Percentile Threshold	0.75-0.87	0.72-0.82
85%-95% Percentile samples / total population	0.096	0.094
Proportion of 85%-95% Percentile samples / sorted sample population	0.65	0.64
95% Percentile Threshold	>0.87	>0.87
>95% Percentile samples / total population	0.051	0.053
Proportion of > 95% Percentile samples / sorted sample population	0.35	0.36

Table S4. Fermentation results for selected mutants and wild type of IDY1 strain, fermentation rate based on CO₂ release calculated based on the logistic growth model, statistical summary of One-way ANOVA of Ethanol Yield at 95% CI compared to WT - P values: 0.1234 (ns), 0.0332 (*), 0.0021 (**), 0.0002 (***), <0.0001 (****).

Strain	rate (h ⁻¹)	Yield (g Ethanol · g biomass ⁻¹)	Average yeast biomass (mg)	Statistical Summary to WT	Ethanol Concentration (% v/v)	Fermentation Efficiency (%)
IDY1-M23	0.144	8.51	17.85	****	6.43	53.69
IDY1-WT	0.147	5.46	30.15	-	6.96	58.16
IDY1-H3	0.122	4.69	30.70	*	6.08	51.40
IDY1-M2	0.144	3.38	45.13	****	6.44	53.83
IDY1-H2	0.113	3.33	44.23	****	6.22	51.99
IDY2-M9	0.128	4.43	36.66	****	6.87	57.47
IDY2-M22	0.105	3.63	39.60	*	6.08	50.85
IDY2-H13	0.109	3.58	41.70	ns	6.31	52.83
IDY2-H23	0.094	3.13	50.03	-	6.63	55.39
IDY2-WT	0.096	2.97	49.20	ns	6.19	51.73

Table S5. List of equipment, vendor and serial number used in autonomous multiplexed sorting.

Component	Vendor	Serial No.
Low-pressure neMESYS pump system	Cetoni	N/A
TREK high-voltage amplifier	Advanced Energy Inc.	PZD700A
Keysight function/arbitrary waveform generator 10 MHz	Keysight Technologies	33210A
Linear DC Power Supply with 4 Channels	GW Instek America Corp.	GPE-4323
Inverted microscope	Olympus	IX73
Vibration-dampening bench	Thorlabs	N/A
Filter block		FOFMS-UV
Multichannel LED light source	Ocean Optics	MCLS 2073
Bandpass filters	Thorlabs	FB450-40 and FL457.9-10
UV LED light source	Thorlabs	M375F2
Hamamatsu ORCA-Flash 4.0	Hamamatsu	N/A
Flame spectrometer	Ocean Optics	N/A
Optical fibers	Thorlabs	FG105UCA, FG200UEP and FG200LCC

Table S6. COMSOL Multiphysics parameters for modeling flow rate and electric field profile of multiplexed sorter device.

Property	Value
Cr Electrical Conductivity	7.9×10^6 [S/m]
Dielectric Thickness SU-8 5	7.0 [μm]
Electrode Gap Width	25 [μm]
HFE 7500 Electrical Conductivity	3×10^{-8} [S/m]
HFE 7500 Oil Relative Permittivity	5.8
PDMS Density	970 [$\text{kg} \cdot \text{m}^{-3}$]
PDMS Electrical Conductivity	4×10^{-13} [S/m]
PDMS Relative Permittivity	2.75
Reference Pressure Level	1 [atm]
Reference Temperature	293.15 [K]
SU8-5 Electrical Conductivity	2.8×10^{-14} [S/m]
Su8-5 Relative Permittivity	4.5

Supplementary Figures

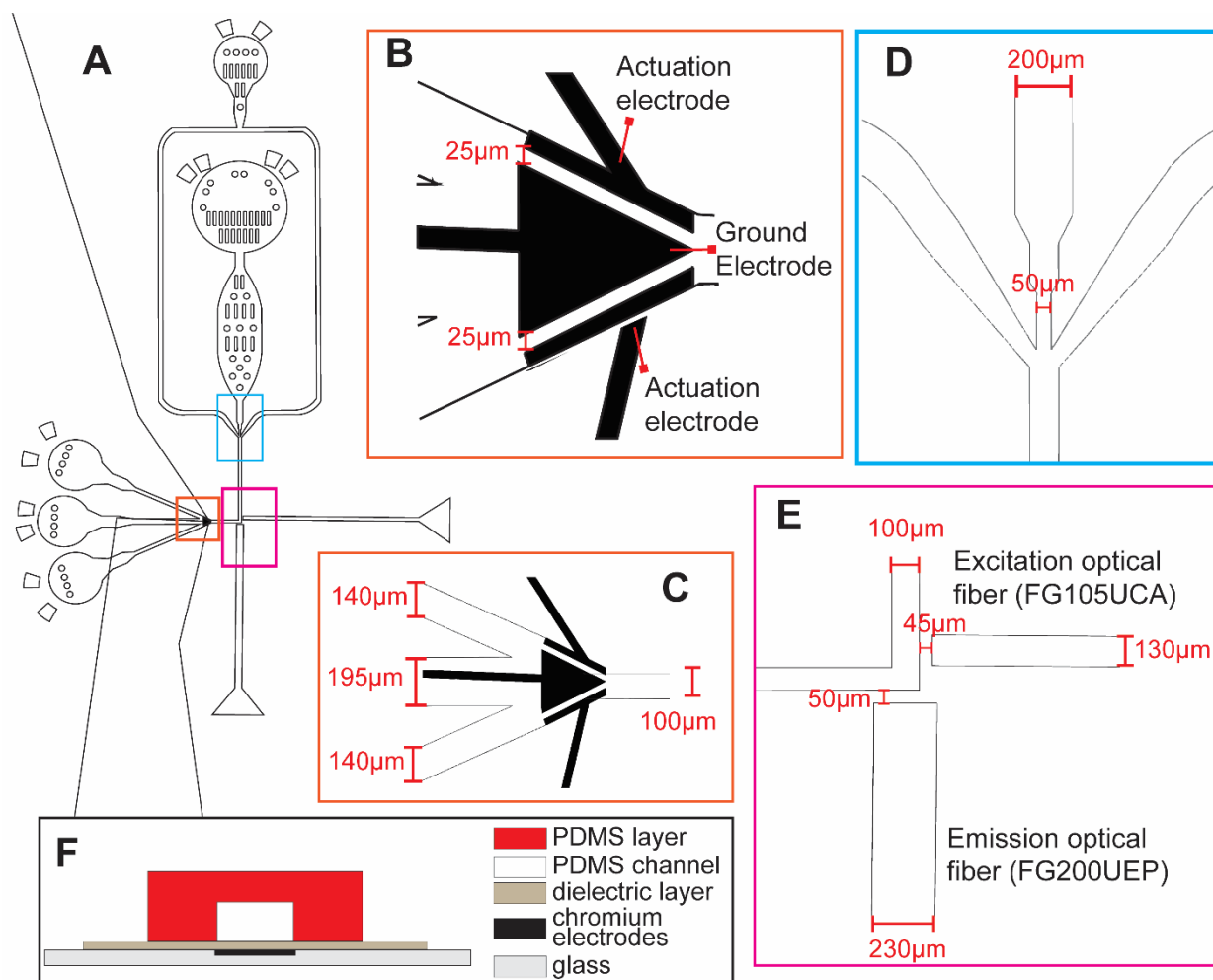


Figure S1. Design of the droplet-digital microfluidic sorter device. A) The overall device which was designed with two inlets (droplets and spacer oil) and three sorting outlets and has three main regions. B) Sorting electrodes configuration showing two actuation electrodes – one for each sorting channel and one ground electrode. The gap between electrodes is 25 μ m. C) Sorting area dimensions with two identical sorting channels and one waste channel with bigger width. D) Dimensions of droplet spacing area – exiting droplet nodule designed with 50 μ m to fit only one droplet based on the sizes from \varnothing 30 – 100 μ m. E) Design of the detection area showing optical fibers channels for excitation \varnothing 105 μ m fiber and \varnothing 200 μ m emission fiber. Emission channel was fabricated with two layers fabrication (\sim 200 μ m height) to fit the optical fiber. F) Device fabrication side view – three main layers (PDMS, dielectric and chromium electrodes).

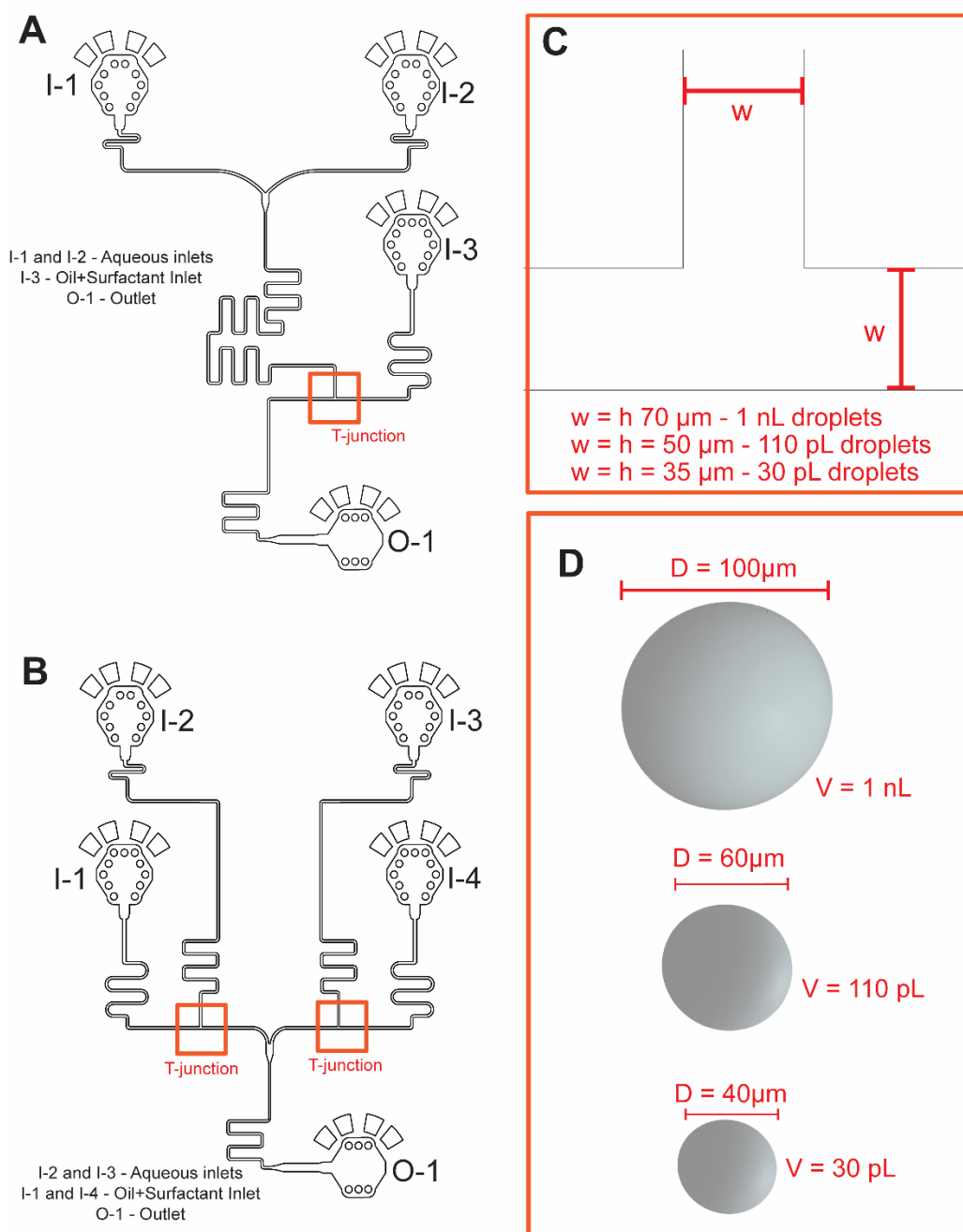


Figure S2. Design and dimensions of droplet generator for different sizes of droplets. A) Design of a single droplet generator with two aqueous inlets to mix fluorescence substrate and cell population for single cell droplet generator using a T-junction design. B) Design of a double droplet generator for characterization of sorter efficiency with two aqueous inlets with individual oil inlets. Design used to make fluorescein and PBS droplets in a single device. C) Dimensions of the T-junction to generate droplets of different sizes (30 pL, 110 pL and 1 nL) – channels were fabricated with height (h) and width (w) with 1:1 ratio. D) 3D simulation comparing the dimensions of the three different droplet sizes used in this work.

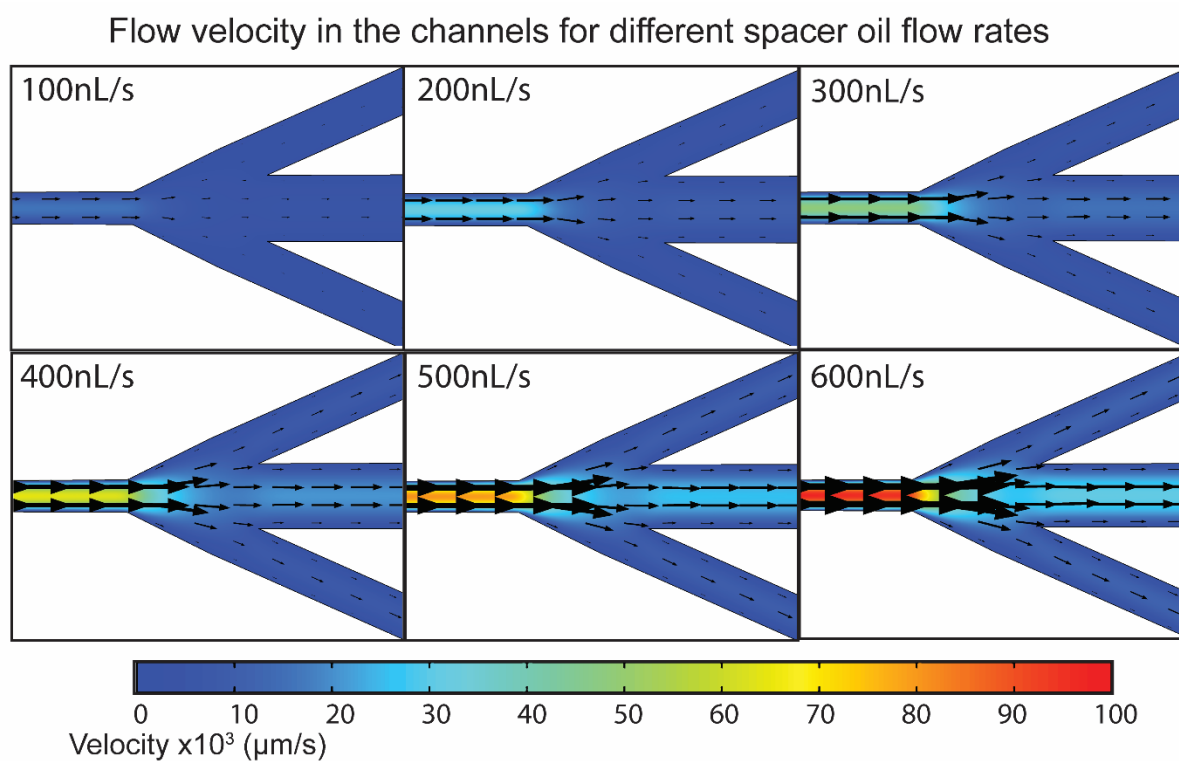


Figure S3 – COMSOL numerical simulations showing the behavior of droplets as they approach the sorting area and are directed toward the waste channel when the electrode deactivated. These simulations illustrate variations in flow velocity patterns influenced by different oil spacer flow rates. Arrows within the simulations highlight the flow's inclination to divert towards channels with lower resistance. The color scheme used in the simulations delineates the velocity patterns within the two sorting and waste channels.

Electric field for different voltage applied to sorting electrode

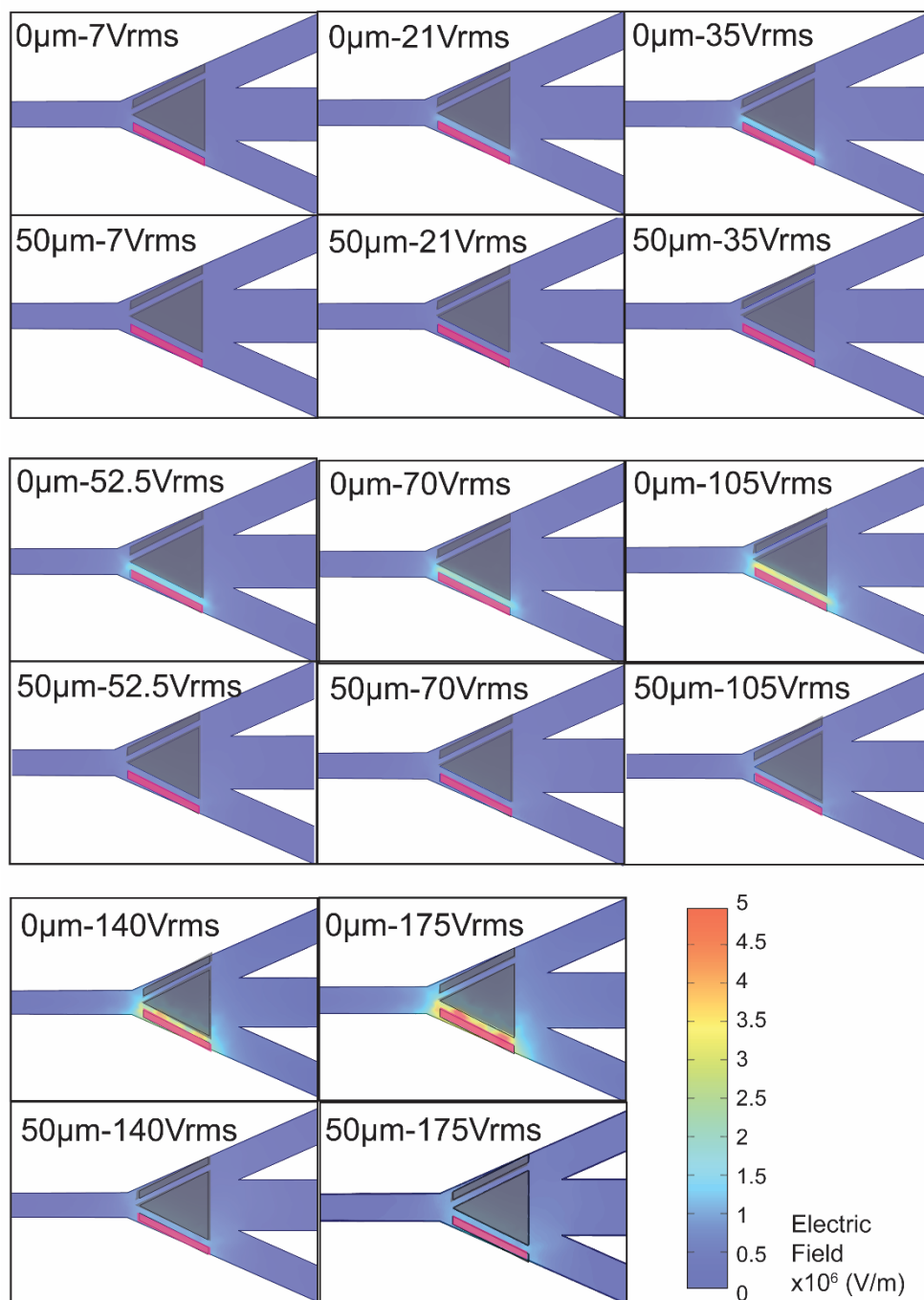


Figure S4 – COMSOL simulation of the electric field above the electrodes. This model includes a channel layer with a PDMS boundary and an HFE 7500 domain, along with a 7 μm thick dielectric layer and three electrode terminals. The simulation presents the electric field strength (measured in V/m) at heights of 0 and 50 μm (above dielectric layer) when the sorting electrode is actuated with different V_{RMS} settings at 15 kHz.

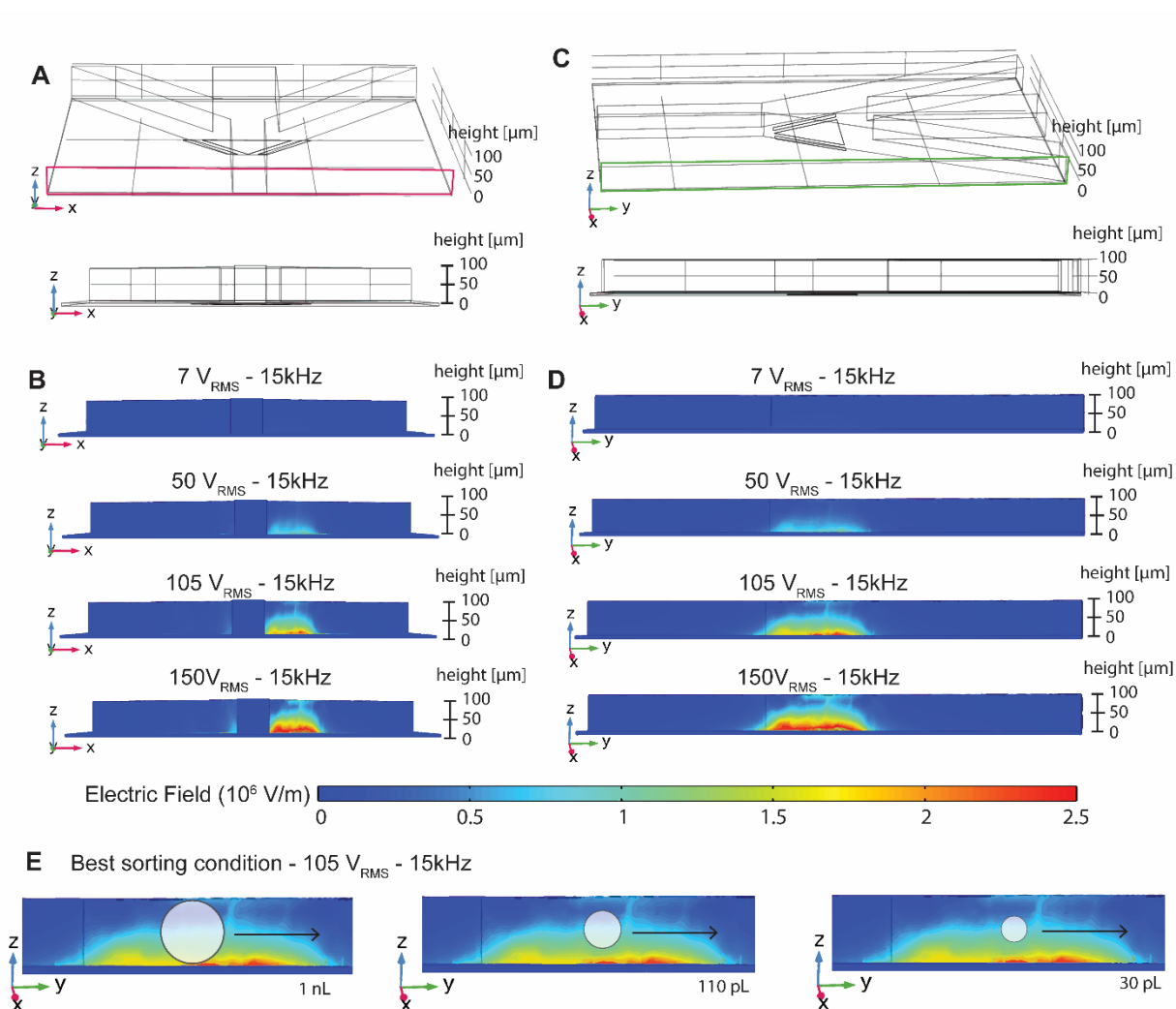


Figure S5 – 3D COMSOL Simulation of Electric Field Strength: A) Schematic and side view in the x-z plane, illustrating the layout of the sorting and waste channels. B) Electric field strength in the x and z planes, adjusted by applying varying potentials. C) Schematic and side view in the y-z plane of the sorting and waste channels. D) Electric field strength in the y and z planes with different potentials applied. This model includes a channel layer with a PDMS boundary and an HFE 7500 domain, a $7 \mu\text{m}$ thick dielectric layer, and three electrode terminals. The simulation details the electric field strength (in V/m) at the entire height of the channels above the dielectric layer when the sorting electrode operates at different V_{RMS} settings at 15 kHz . E) Side view comparison of the electric field in the sorting area relative to droplets of different sizes, demonstrating field strength perpendicularly with the droplets flow (black arrow).

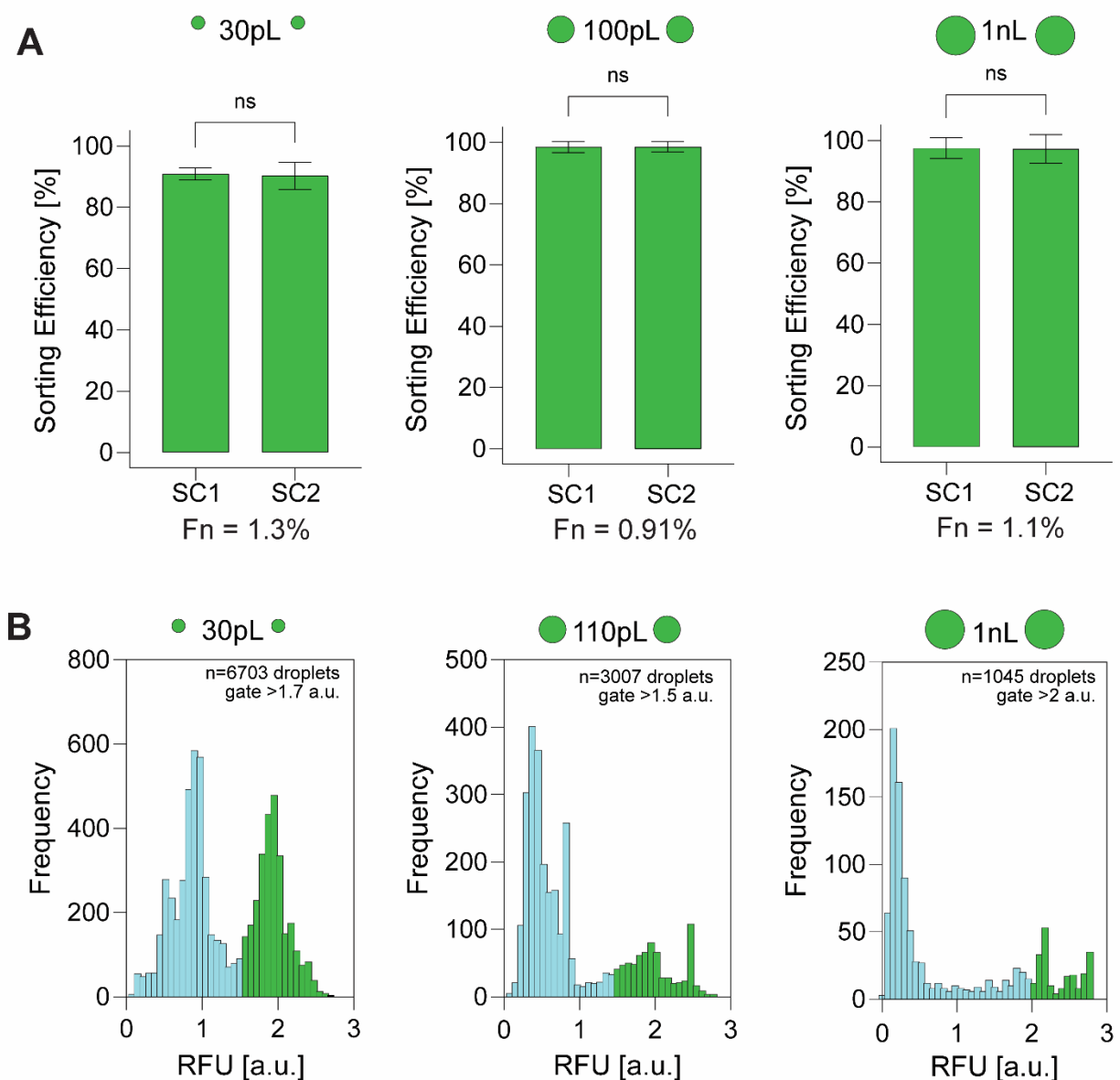


Figure S6. Sorter Efficiency as a Binary Sorter to Test Design Efficiency. A) Comparison of sorting of 1mM fluorescein droplets mixed with PBS droplets between two different sorting channels. Efficiency is quantified by the proportion of fluorescent droplets in each respective sorting channel (SC1 or SC2) relative to the total number of droplets in that channel. False negatives (Fn) represent the percentage of fluorescent droplets in the waste channel. Error bars representing standard deviation $N > 3$, Unpaired t-test at 95% CI - P values: 0.1234 (ns), 0.0332 (*), 0.0021 (**), 0.0002 (***), < 0.0001 (****). B) Fluorescence histograms used for gating in the autonomous sorting of three different droplet sizes.

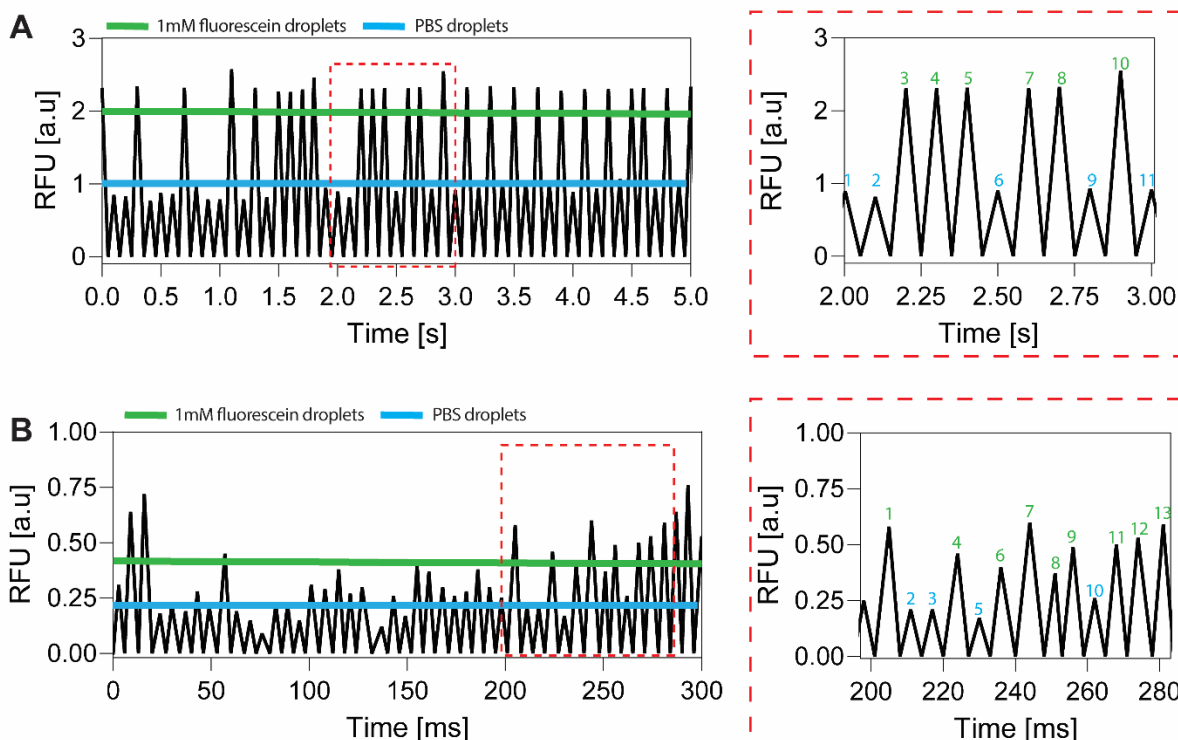


Figure S7 – Time series of fluorescence detection of droplets of 30 pL mixture of 1 mM fluorescein and PBS droplets (1:1 ratio). A) Graph showing detection of 10 Hz droplet detection with $0.3 \text{ nL}\cdot\text{s}^{-1}$ droplet re-injection flow rate and $200 \text{ nL}\cdot\text{s}^{-1}$ spacer oil flow rate. Expanded view showing peaks detected overtime (PBS droplets $< 1 \text{ a.u.}$ – blue line, and 1 mM fluorescein $> 2 \text{ a.u.}$ – green line). B) Graph showing detection of 160 Hz droplet detection with $3 \text{ nL}\cdot\text{s}^{-1}$ droplet re-injection flow rate and $300 \text{ nL}\cdot\text{s}^{-1}$ spacer oil flow rate. Expanded view showing peaks detected overtime (PBS droplets $< 0.25 \text{ a.u.}$ – blue line, and 1 mM fluorescein $> 0.4 \text{ a.u.}$ – green line).

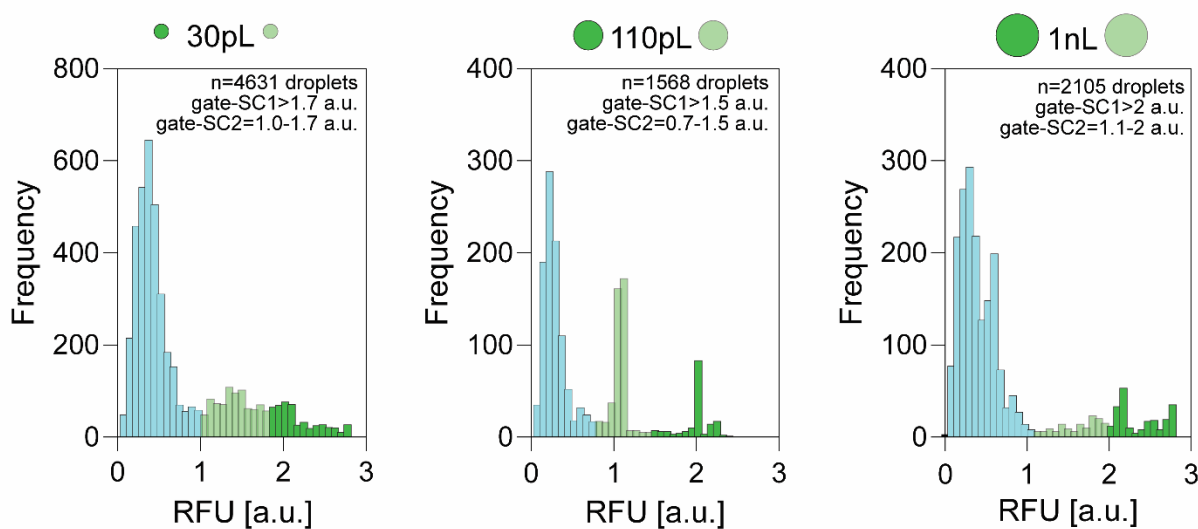


Figure S8. Fluorescence histograms used for gating the autonomous multiplexed sorting of 1 mM fluorescein (dark green), 0.1 mM (light green) and PBS (blue) droplets mixture of different droplet sizes.

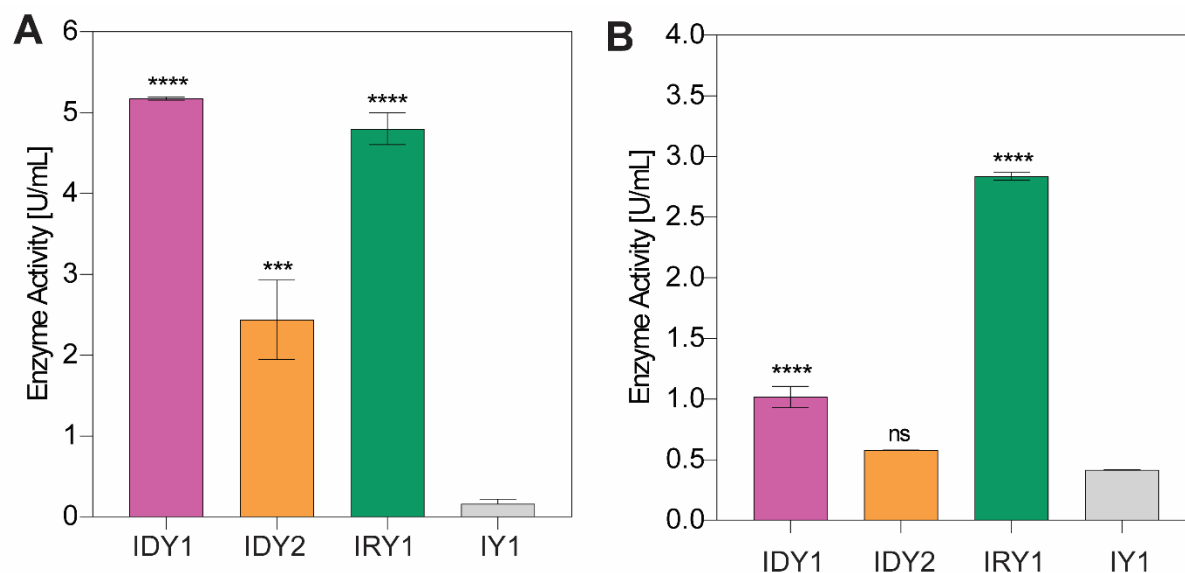


Figure S9. Enzyme activity of diastatic yeast strains compared to positive and negative glucoamylase controls. A) Enzymatic assay performed using 4-Nitrophenyl β -D-maltoside as substrate. B) Enzymatic assay performed using 4-Nitrophenyl α -D-glucopyranoside. Error bars representing standard error N=3, One-way ANOVA at 95% CI compared to IY1 - P values: 0.1234 (ns), 0.0332 (*), 0.0021 (**), 0.0002 (***), <0.0001 (****).

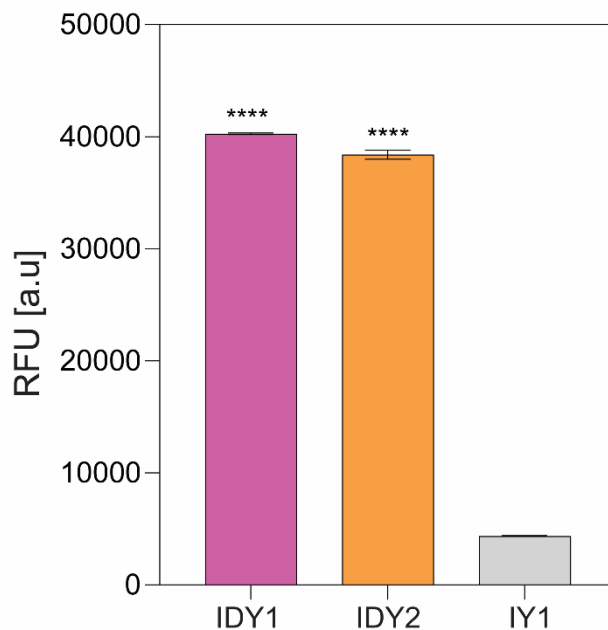


Figure S10. Enzyme activity of diastatic yeast strains compared to the negative glucoamylase controls. Enzymatic assay performed using 4-Methylumbelliferyl- α -D-glucopyranoside with reaction stopped with buffer pH 11. Error bars representing standard error N=3, One-way ANOVA at 95% CI compared to IY1 - P values: 0.1234 (ns), 0.0332 (*), 0.0021 (**), 0.0002 (***), <0.0001 (****).

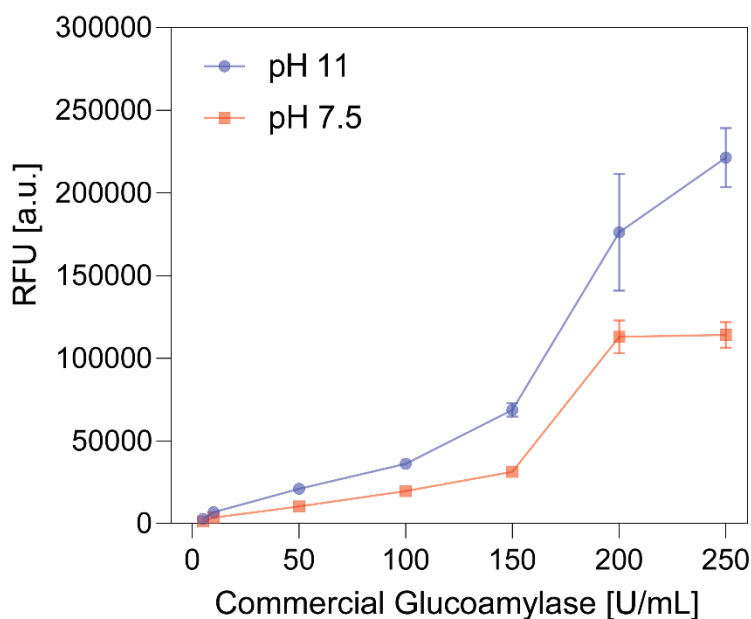


Figure S11. Enzyme activity of commercial glucoamylase performed using 4-Methylumbelliferyl- α -D-glucopyranoside with reaction stopped with buffer pH 11 and pH 7.5. Error bars representing standard deviation N=3.

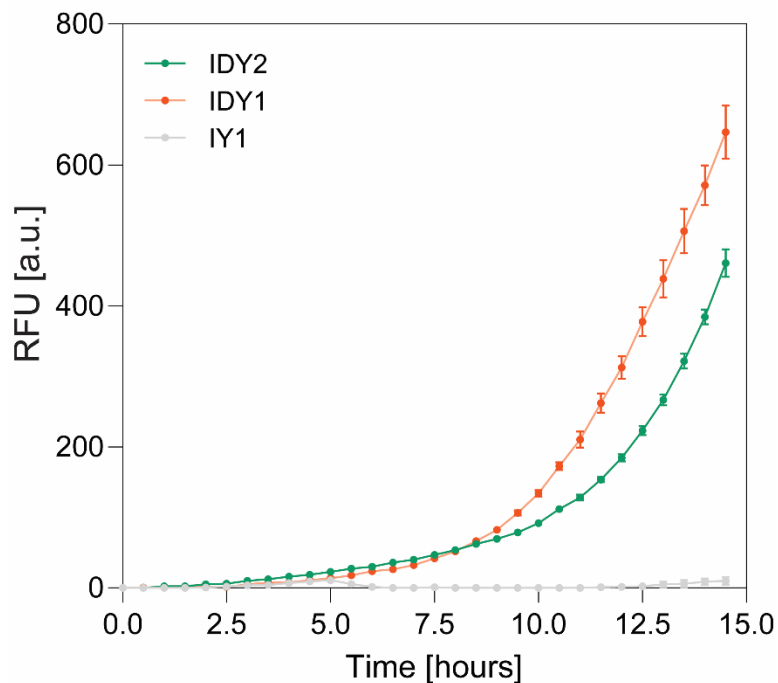


Figure S12. Overnight enzyme activity of diastatic yeast strains compared to the negative glucoamylase controls using 4-Methylumbelliferyl- α -D-glucopyranoside pH 7.5. Fluorescence was taken while yeast culture growth in YPD media. Error bars representing standard deviation N=3.

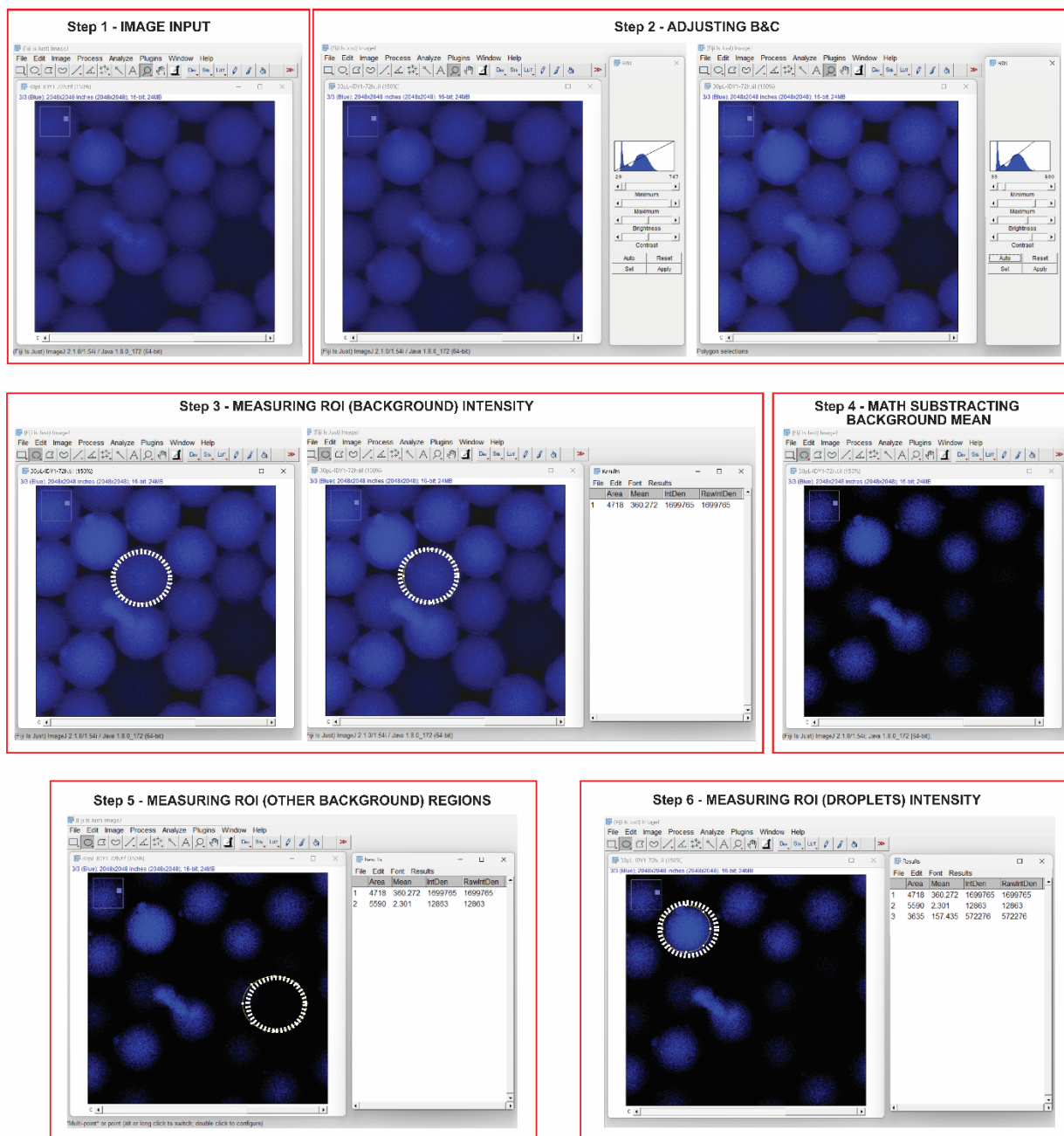


Figure S13. Analysis Workflow for Measuring Fluorescence Intensity in Droplets. The raw fluorescence microscopy image is loaded into the analysis software (Step 1) and adjusted for brightness and contrast (Step 2). A background ROI is selected, and its mean intensity is measured (Step 3). This mean background intensity is subtracted from the entire image (Step 4). Additional background ROIs are measured for consistency (Step 5). Finally, ROIs within the droplets are measured for fluorescence intensity, corrected by subtracting the background mean (Step 6).

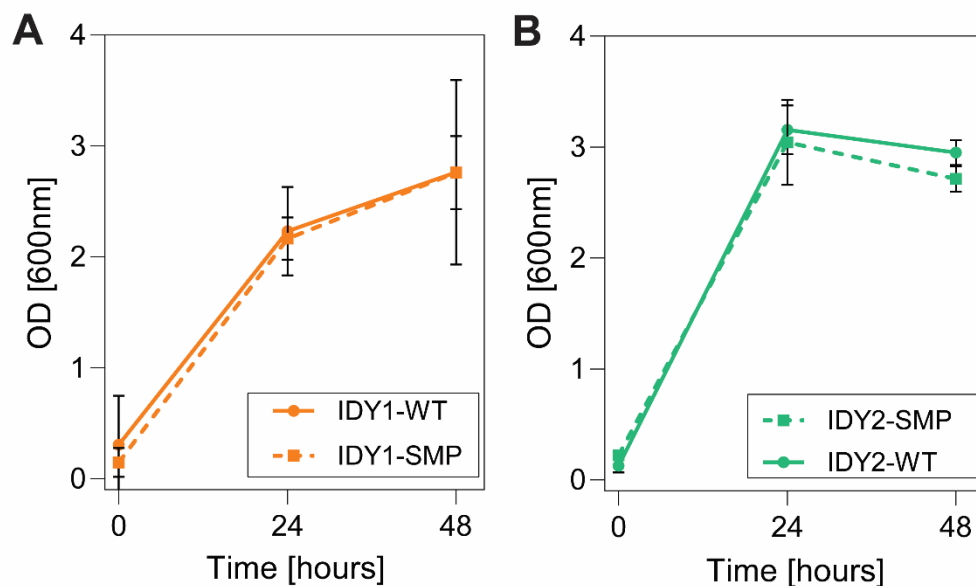


Figure S14. Comparison of maltodextrin growth of self-mated population (SMP) and the wild type (WT) by measuring optical density (OD). A) IDY1 strains. B) IDY2 strains. Error bars representing standard deviation N=6.

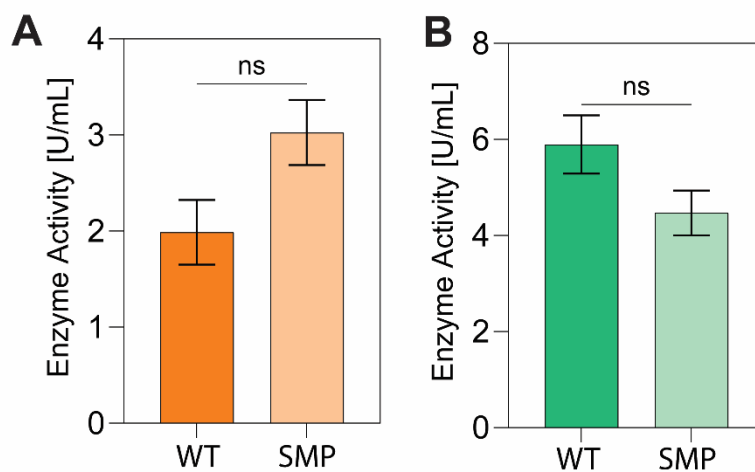


Figure S15. Comparison of enzyme activity of glucoamylase produced by a self-mated population (SMP) and the wild type (WT). A) IDY1 strains. B) IDY2 strains. Unpaired t-test at 95% CI - P values: 0.1234 (ns), 0.0332 (*), 0.0021 (**), 0.0002 (***), <0.0001 (****). Error bars representing standard error N=3.

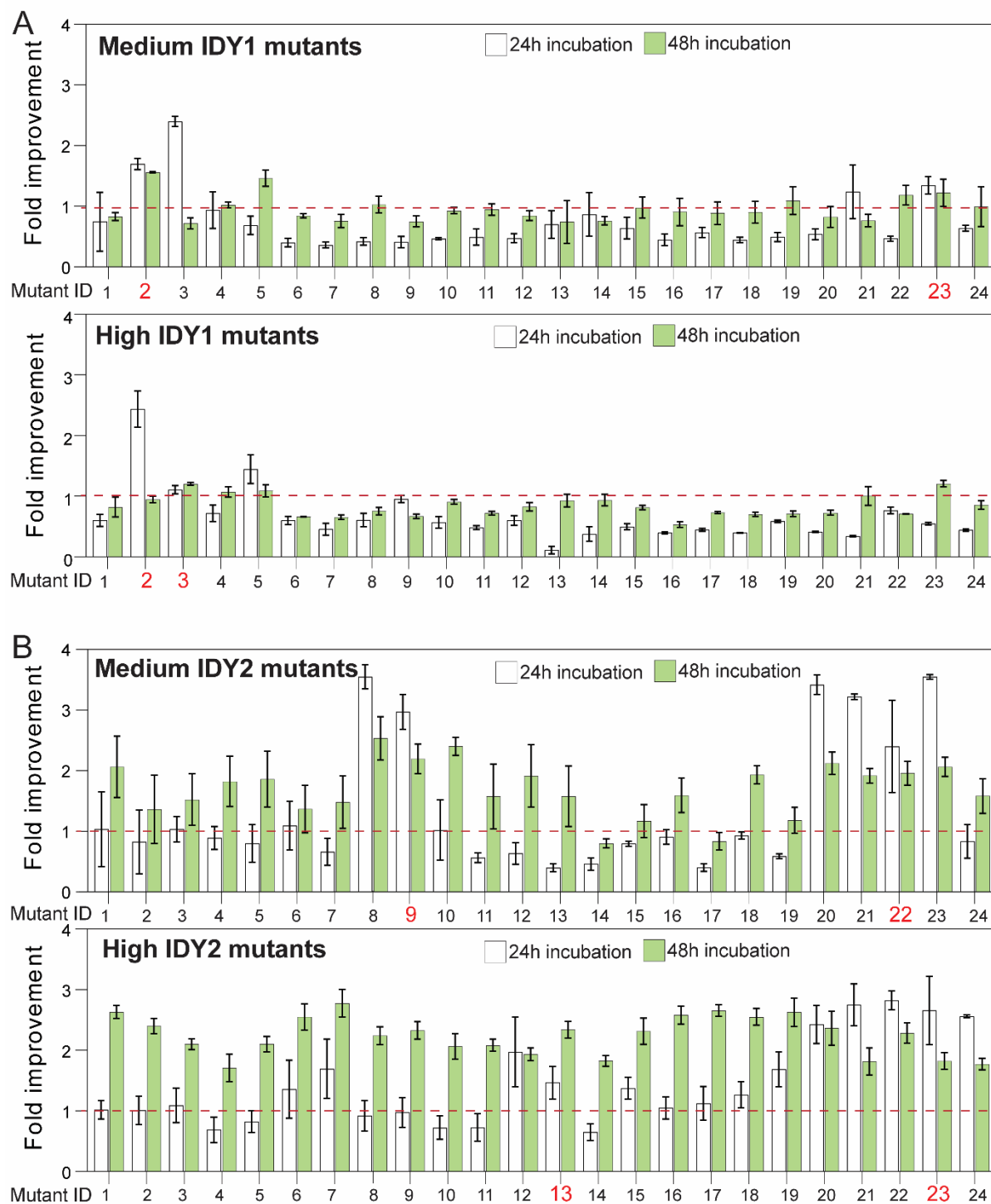


Figure S16. Fold improvement of IDY1 and IDY2 mutant strains compared to wild type under two incubation periods: 24 hours (white bars) and 48 hours (green bars) in maltodextrin media. A) Medium and High IDY1 mutants showing the fold improvement for growth in maltodextrin. B) Medium and High IDY2 mutants showing the fold improvement for growth in maltodextrin. Error bars represent the standard error. The red dashed line marks the wild type, and red highlighted mutants are the selected ones for further fermentation experiments.

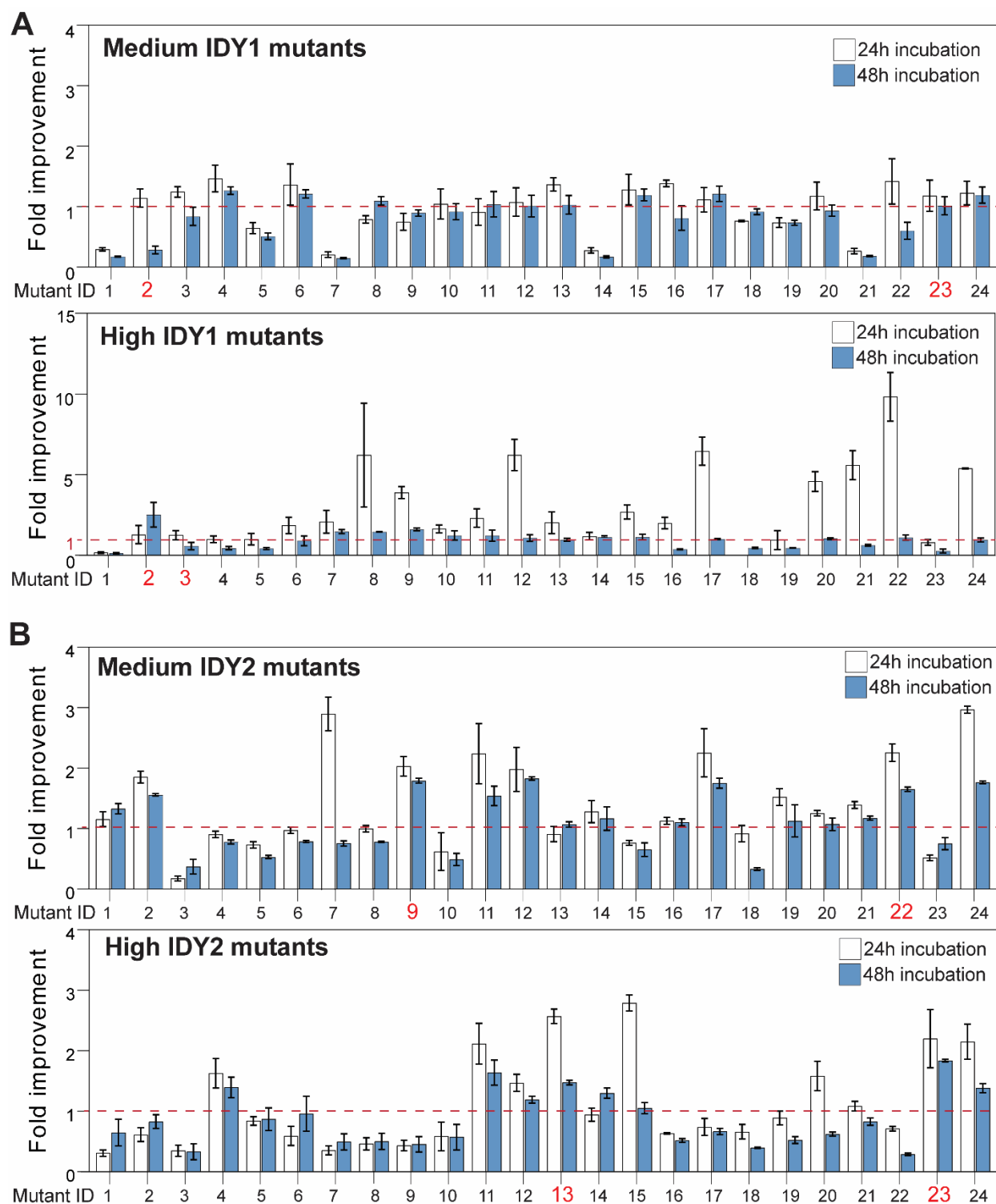


Figure S17. Fold improvement of IDY1 and IDY2 mutant strains compared to wild type under two incubation periods: 24 hours (white bars) and 48 hours (green bars) for glucoamylase activity. A) Medium and High IDY1 mutants showing the fold improvement for enzyme activity. B) Medium and High IDY2 mutants showing the fold improvement for enzyme activity. Error bars represent the standard error. The red dashed line marks the wild type, and red highlighted mutants are the selected ones for further fermentation experiments.

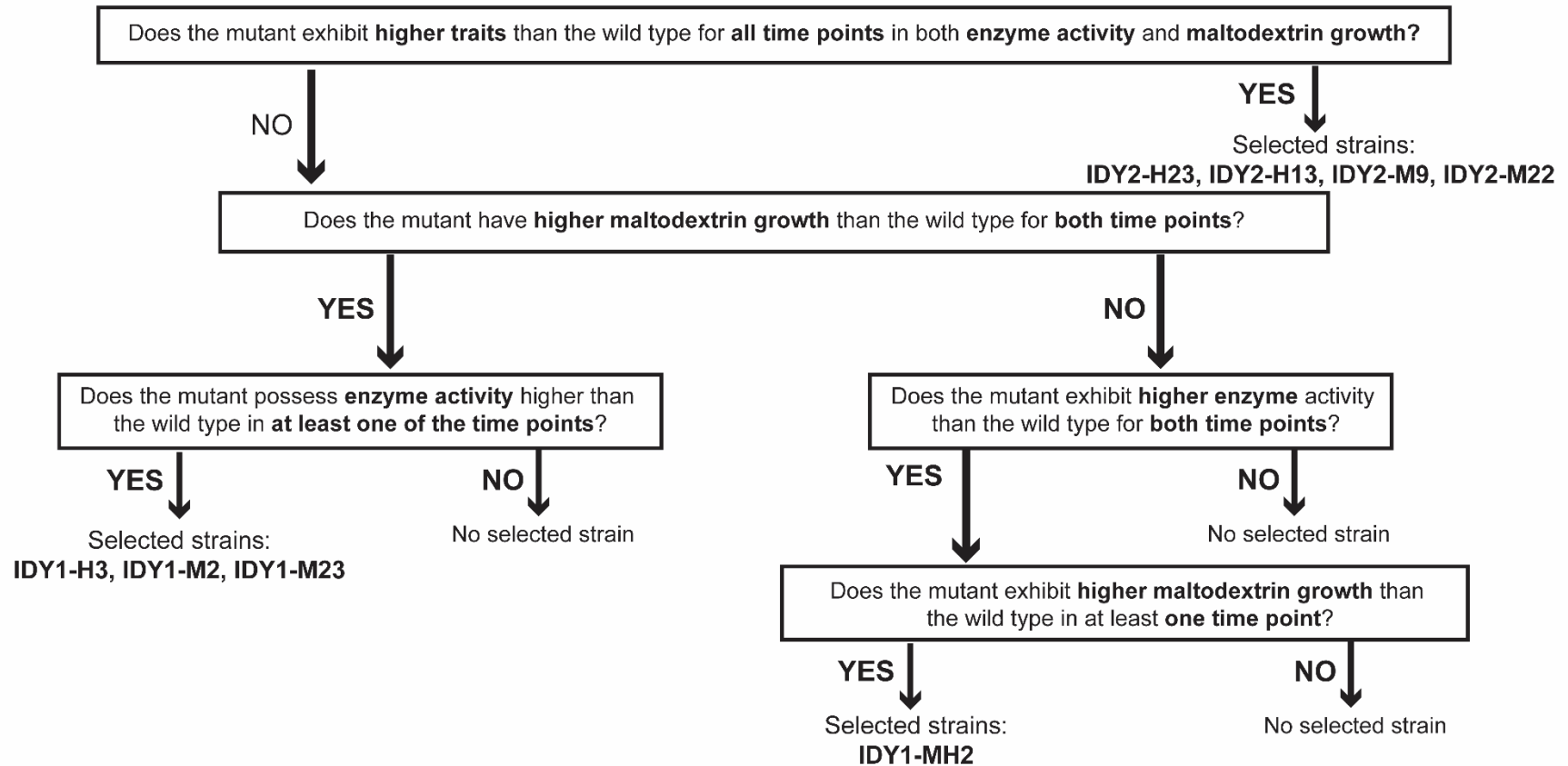


Figure S18. Decision tree for selecting mutant strains based on enzyme activity and maltodextrin growth. This decision tree outlines the selection criteria for mutant strains exhibiting higher traits compared to the wild type after sorted into two different populations: mid-fluorescence (M) and high-fluorescence (H).

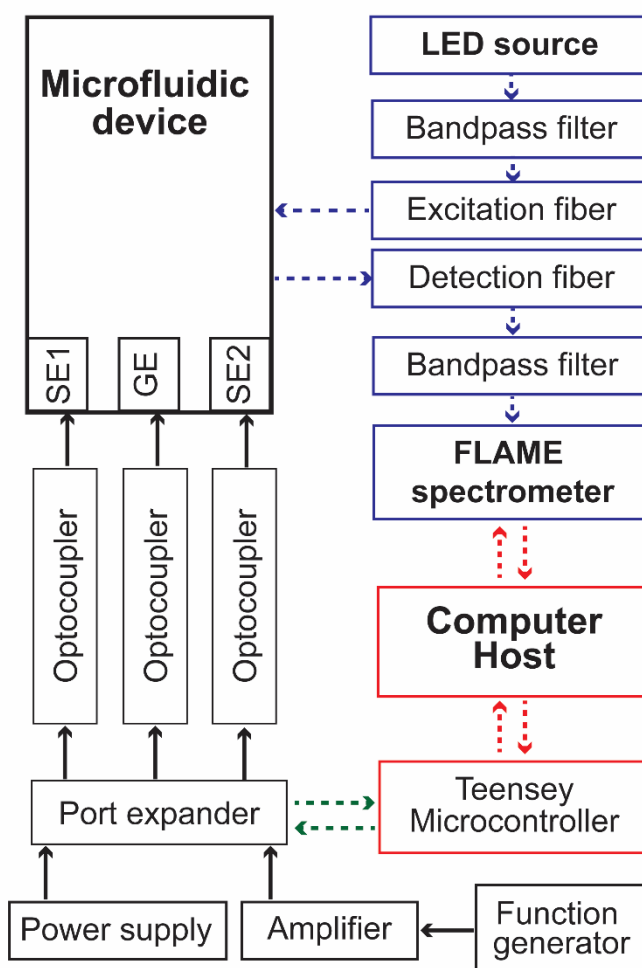


Figure S19. Software and Hardware block diagram. This diagram illustrates the electronic control system for the droplet-digital microfluidic sorter device. Optical fluorescence intensity data is captured and relayed to a flame spectrometer, which converts the readings into Relative Fluorescence Units (RFU) on a host computer using "uFlow control" software (<https://bitbucket.org/shihmicrolab/fahmadi2023uflowcontrol>). Upon reaching the preset fluorescence threshold, the software transmits a signal through a Teensy microcontroller to a port expander, which in turn actuates the sorting electrodes via optocouplers to control droplet sorting. Red dotted lines indicate USB connections, green dotted lines represent I2C connections, blue dotted lines show optical fiber connections, and solid black lines to electrical wire connections. Autonomous sorting software available to download at (https://bitbucket.org/shihmicrolab/f_ahmadi_2023_uflowcontrol).^[2]

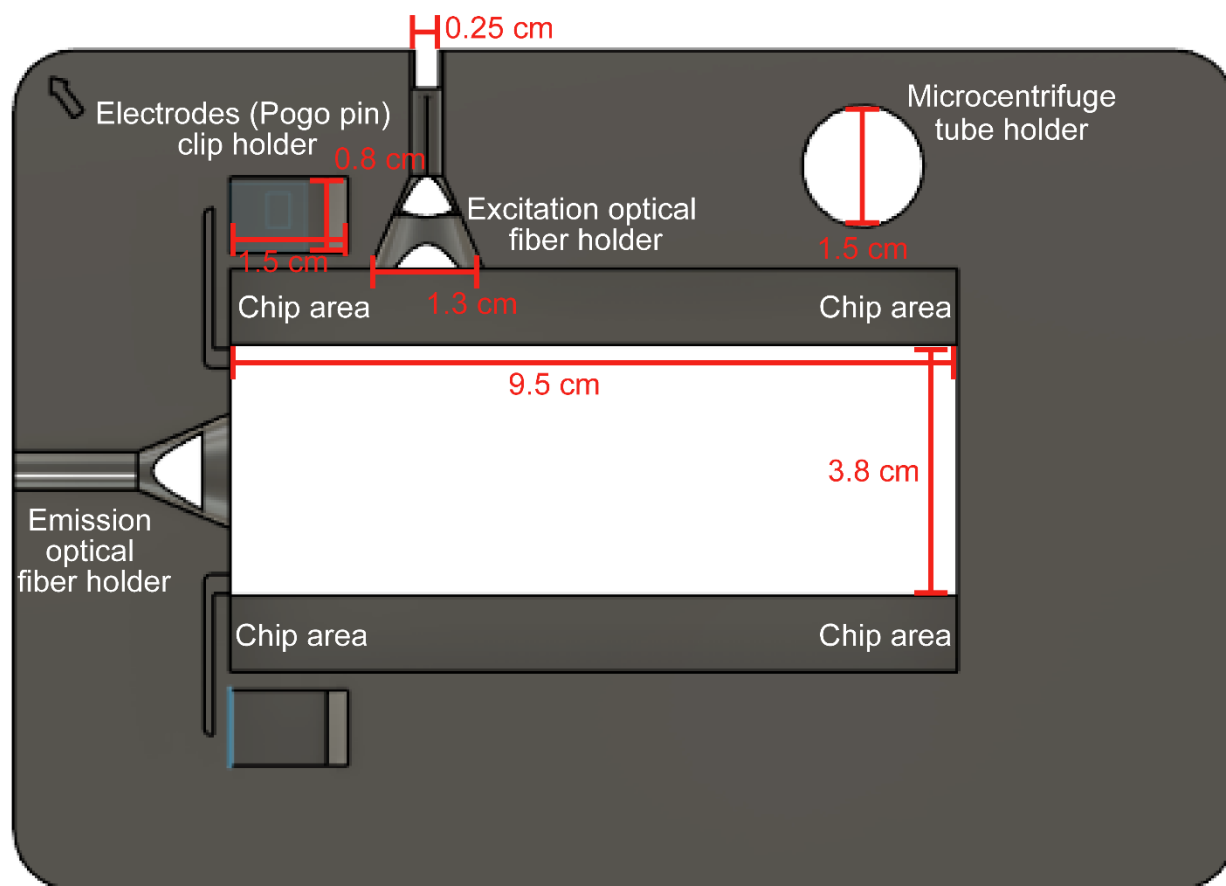


Figure S20. 3D Printed Chip Holder. Diagram illustrating a chip holder designed for accommodating various components essential for multiplexed sorting experiments. The central rectangular area labeled "Chip area" is where the droplet-digital sorter is placed. Excitation optical fiber holder and "Emission optical fiber holder are designed to facilitate the positioning of optical fibers for excitation and emission detection, respectively. The Electrodes (Pogo pin) clip holder is designated for securing electrodes. Microcentrifuge tube holder is included for holding microcentrifuge tubes, which could be used for sample preparation or collection. The layout ensures that all components are securely held in place, providing a stable setup for experimental procedures.

Supplementary References

- [1] S. C. C. Shih, G. Goyal, P. W. Kim, N. Koutsoubelis, J. D. Keasling, P. D. Adams, N. J. Hillson, A. K. Singh, *ACS Synth. Biol.* **2015**, *4*, 1151–1164.
- [2] F. Ahmadi, H. Tran, N. Letourneau, S. R. Little, A. Fortin, A. N. Moraitis, S. C. C. Shih, *Small* **2024**, *20*, 2308950.